Hybrid Polymer-Liquid Electrolytes and Their Interactions with Electrode Materials

ChemElectroChem

Research Article
doi.org/10.1002/celc.202400561

Chemistry Europe
European Chemical Societies Publishing

www.chemelectrochem.org

Hybrid Polymer-Liquid Electrolytes and Their Interactions with Electrode Materials

Martina Cattaruzza,[b] Mats Johansson,[b] Göran Lindbergh,[c] and Fang Liu*[a]

To address the increasing demand for efficient, safe, and sustainable energy storage solutions in the transition towards renewable energy and electrified society, this study explores hybrid polymer-liquid electrolytes (HEs) as a novel solution to overcome challenges of traditional liquid electrolytes used in lithium-ion batteries (LIBs). Particularly, the research is focused on polymerization-induced phase separation (PIPS) synthesized HEs with distinct phase-separated systems, where an ion-conducting liquid phase percolates the macropores and mesopores within the formed thermoset solid phase. This study investigates the feasibility of using HEs with commercial cathodes and highlights their respective merits and challenges. The feasibility of infusing and forming HEs in commercial cathodes via PIPS within both micron-sized and nano-sized confined spaces is proved. By incorporating these HE-infused electrodes into half-cell configurations, the study proves that the HEs are compatible with common cathodes, and they exhibit energy density comparable with traditional systems with liquid electrolyte.

Introduction

Lithium-ion batteries (LIBs) are pivotal in modern energy storage, powering applications from portable electronics to electric vehicles. Their high energy density, long cycle life, and low self-discharge rate make them a leading choice for energy storage.[1–4] In a battery, the primary components – cathode, anode, and electrolyte – must work in synergy to maintain stability, efficiency, and safety.[5–8] The cathode typically comprises the active material, conductive additives (such as carbon black), and a binder (such as PVDF) to hold the components together. Two widely used commercial active cathode materials are nickel manganese cobalt oxide (NMC) and lithium iron phosphate (LFP).[5] The voids between the active particles are filled with liquid electrolyte. Interphases between the electrolyte and electrode material play a critical role in lithium-ion batteries, serving as primary sites for electrochemical processes that govern battery operation. Through electrode-electrolyte interfaces, lithium ions reversibly intercalate and deintercalate during charge-discharge cycles, inducing volume changes, which are critical for the structural integrity and long-term performance of the electrode material.[9] Volume fluctuations may induce strain and stress in the electrode[10] and increase internal resistances. The phenomenon impacts charge-transfer kinetics, often reducing battery efficiency and leading to premature battery failure. Such alterations are particularly relevant for cathode materials, as their high electrode potentials (i.e. severe oxidizing conditions) make them more susceptible to challenging interfacial dynamics.[11]

A major challenge when it comes to conventional LIB is the liquid electrolyte used, which poses safety risks due to leakage, flammability, and potential electrolyte decomposition.[8,12] Finding alternatives is crucial for advancing battery safety and performance. Polymer electrolytes represent a promising avenue in LIB research, offering potential solutions to the limitations associated with traditional liquid electrolytes. One key advantage of polymer electrolytes is their enhanced safety compared to conventional liquid electrolytes. An example is gel polymer electrolytes (GPEs), which consist of a liquid phase that swells a polymer phase, forming a gel-like structure where the risk of leakages is significantly reduced.[13] Another type of polymer electrolyte is the hybrid polymer-liquid electrolyte (HE). HEs consist of a bicontinuous phase-separated system in which a cross-linked polymer matrix encapsulates a liquid phase containing conventional lithium salts and organic solvents. The liquid phase allows efficient transport of lithium ions within the electrolyte while polymer matrices provide structural integrity minimizing the risks of leakages. HEs exhibit a highly porous morphology, where the liquid phase forms an interconnected pathway throughout the material, ensuring efficient ion transport. Our recent studies, utilizing nuclear magnetic resonance (NMR), have revealed that this structure includes pores ranging

[a] Prof. F. Liu
Division of Materials and Manufacture, Department of Industrial and Materials Science
Chalmers University of Technology
SE-412 96 Gothenburg, Sweden
E-mail: fang.liu@chalmers.se

[b] M. Cattaruzza, M. Johansson
Division of Coating Technology, Department of Fiber and Polymer Technology
KTH Royal Institute of Technology
SE-100 44 Stockholm, Sweden

[c] G. Lindbergh
Göran Lindbergh
Division of Applied Electrochemistry, Department of Chemical Engineering
KTH Royal Institute of Technology
SE-100 44 Stockholm, Sweden

Supporting information for this article is available on the WWW under https://doi.org/10.1002/celc.202400561

from micropores (< 2 nm) to mesopores (2–50 nm), which play a role in the accessibility and mobility of lithium ions.[14] This morphology plays a critical role in achieving high ionic conductivity, with measured values exceeding 10^{-4} S*cm^{-1} at room temperature. These electrolytes can be synthesized using a process known as polymerization-induced phase separation (PIPS)[15–17] wherein the phase separation occurs concurrently with the polymerization process due to the different solubilities of the monomer and the resulting polymer in the liquid electrolyte phase. This process creates a heterogeneous interconnected structure that allows the liquid and polymer phases to maintain distinct but complementary functions. Lodge et al. pioneered the use of PIPS as a method for creating heterogeneous electrolytes through stepwise polymerizing systems in conjunction with ionic liquids.[18–21]

Beyond addressing some of the limitations associated with the use of traditional liquid electrolytes, HEs have the potential to serve as multifunctional materials in battery applications. The conventional method for producing LIB electrode materials involves mixing the electrode components – active material, conductive additive and binder – with a solvent or a blend of solvents to form a uniform slurry.[22] HEs could realize both binder and electrolyte functions with a single PIPS step, simplifying production and potentially reducing environmental impact by minimizing the need for fluorinated binders and harmful solvents.[23]

HEs have shown promise in structural composite batteries made from carbon fibers.[24–27] However, to our knowledge, their application in commercial electrodes has not yet been investigated, and their compatibility with commercial cathodes remains largely underexplored. In this proof-of-concept study, we evaluate HEs synthesized via PIPS for their integration into commercial LFP and NMC cathodes, assessing their electrochemical stability and performance in operational half-cells.

Experimental

Materials

The cathode with lithium iron phosphate – $LiFePO_4$ (LFP) was purchased from Customcells Holding GmbH with 90% of active material content, mass loading = 14.8 mg/cm^2, specific capacity = 150 mAh/g, nominal voltage = 3.4 V vs Li/Li$^+$, area capacity = 2 mAh/cm^2 (+/−0.1 mAh/cm^2). The cathode with lithium nickel manganese cobalt oxide – $LiNi_{0.8}Mn_{0.1}Co_{0.1}O_2$ (NMC 811) was purchased from Customcells Holding GmbH with 95% of active material content, mass loading = 21.1 mg/cm^2, specific capacity = 175 mAh/g, nominal voltage = 3.7 V vs Li/Li+, area capacity = 3.5 mAh/cm^2 (+/−0.1 mAh/cm^2). Both electrodes were single side coated on an aluminum current collector, which is 20 μm thick. The commercial liquid electrolyte, consisting of 1 M LiTFSI in a 1:1 v/v mixture of ethylene carbonate (EC) and propylene carbonate (PC) with a purity of 99.9% in a 1 L quantity, was purchased from Solvionic. Additionally, the thermal initiator 2,2′-azobis (2-methylpropionitrile) (AIBN) was purchased from Sigma-Aldrich. The monomer, bisphenol A ethoxylate dimethacrylate (BPAMA) with a molecular weight of 540 g/mol, was supplied by Sartomer, part of the Arkema Group. All materials were utilized as received.

Cells Manufacturing

HE-impregnated LFP and NMC electrodes were prepared using vacuum infusion. The cathode materials were trimmed into approximately 15 mm×100 mm strips and taped onto a 60 mm×180 mm glass plate. The electrodes were then covered with a release film (a perforated polyethylene film) and breather fabric (a distribution medium of coarse polyester felt cloth). The entire setup was vacuum sealed with rubber tape and subsequently dried in a vacuum oven at 60 °C for 24 hours. The HE resin was prepared in the glovebox in dry argon atmosphere (< 1 ppm of H_2O, < 1 ppm of O_2) by mixing the commercial electrolyte with the monomer BPAMA and the initiator AIBN. The AIBN content was 1 wt% relative to the monomer weight, and the liquid electrolyte content was either 45 or 50 wt% of the total weight. After sealing the mixture with a septum, the resin was infused into the dried infusion setup with commercial electrodes outside the glovebox. Once the infusion was completed, the samples were thermally cured at 90 °C for 45 min. After curing, the vacuum bag setup was moved into the glovebox where the cathode lamina was extracted and sliced into two infused electrodes (approximately 15 mm×30 mm). Each infused electrode was subsequently placed into a pouch cell (70 mm×70 mm). A lithium metal foil was used as the counter electrode with a nickel current collector. A 250 μm Whatman glass-microfiber filter was used as separator between the electrodes. To wet the separator and ensure ionic conduction, and possibly replenish electrolyte lost during sample handling, about 300 μL of additional liquid electrolyte was added. Henceforth, the prepared HE-infused electrodes are denoted as HE-xxwt%-LFP and HE-xxwt%-NMC where xx represents the liquid electrolyte content percentage (45 or 50).

For comparison, reference samples of commercial LFP and NMC cathodes were similarly assembled into half cells with a lithium metal counter electrode, a nickel current collector, a Whatman glass-microfiber filter as the separator, and approximately 300 μL of liquid electrolyte.

Morphology Characterization

To investigate the morphology and microstructure of the HE-infused electrodes, the cells were first dissembled and then dried at 60 °C in a vacuum oven for 24 hours to eliminate the liquid electrolyte solvents. Subsequently, HE-infused electrode samples were cut (approximately 5 mm wide) and glued to a piece of Si wafer of similar size, which provides a perfectly flat mask for high-quality polishing of the cross-sectional surface using broad ion beam (BIB). A BIB tool, Leica EM TIC 3X triple ion-beam cutter, was used to mill large (up to 1 mm wide) finely polished cross-sectional surfaces for scanning electron microscopy (SEM) analysis. The BIB sample preparation method can prevent artifacts that usually occur under cryo-fracturing. To minimize ion damage and thermal effects, the argon ion source was set at an energy of 6–6.5 kV. A Zeiss Ultra 55 FEG SEM equipped with a field emission electron gun was used to acquire SEM micrographs. An accelerating voltage of 1 kV was used to reduce charging effects, and a working distance of 3–4 mm was used to record high-resolution images with an in-lens secondary electron detector. Reference samples of pristine, non-infused LFP and NMC cathodes were also prepared and analyzed in the same way for comparison.

Galvanostatic Cycling

The HE-infused electrode half-cells were galvanostatically cycled between 2.6–3.9 V vs Li/ Li$^+$ for LFP and 3.1–4.1 V vs Li/ Li$^+$ for NMC using a Neware CT-4008T-5V10 mA-164 battery tester at

ambient temperature. For this proof-of-concept study, these voltage ranges were based on the electrode suppliers' data sheets and used to evaluate the compatibility of the HEs in half-cells. In future studies, broader potential ranges and long-term cycling may be explored to fully assess performance under varied conditions. To ensure slow interphase formation for morphological studies, the first 10 cycles used low current densities of 6.75 mA/g for LFP and 8.32 mA/g for NMC, corresponding to a C-rate of C/20. During a second stage, the LFP samples underwent galvanostatic cycling for a preliminary capacity retention test over 20 cycles. The applied current densities were 13.5 mA/g, 27 mA/g and 67.5 mA/g, corresponding to a C-rate of C/10, C/5 and C/2, respectively. The capacities were calculated based on the nominal areal capacity of the commercial electrodes. Reference samples of non-infused pristine LFP and NMC with 1 M LiTFSI in EC:PC 1:1 v/v liquid electrolyte were also tested in the same way for comparison.

Results and Discussion

Infusion and PIPS in Electrodes

The success of the infusion of the HE precursors and subsequent polymerization via PIPS in the commercial electrodes, both for LFP and NMC, is demonstrated by SEM. A comparison between the non-infused pristine LFP sample and HE-50 wt%-LFP before cycling is shown in Figure 1. The morphology of pristine LFP consists of well-defined nanosized particles which are tightly packed and separated by nano- or micro-sized voids. In the HE-infused LFP electrode with 50 wt% liquid electrolyte content, the entire void spaces are filled with HE comprising a porous structure with micro- to mesopores, which are similar to what observed in previous studies on bulk HE samples.[14,28] The micrographs demonstrate that the HE precursors can be effectively infused into the voids of the electrode and incorporated between the electrode active particles.

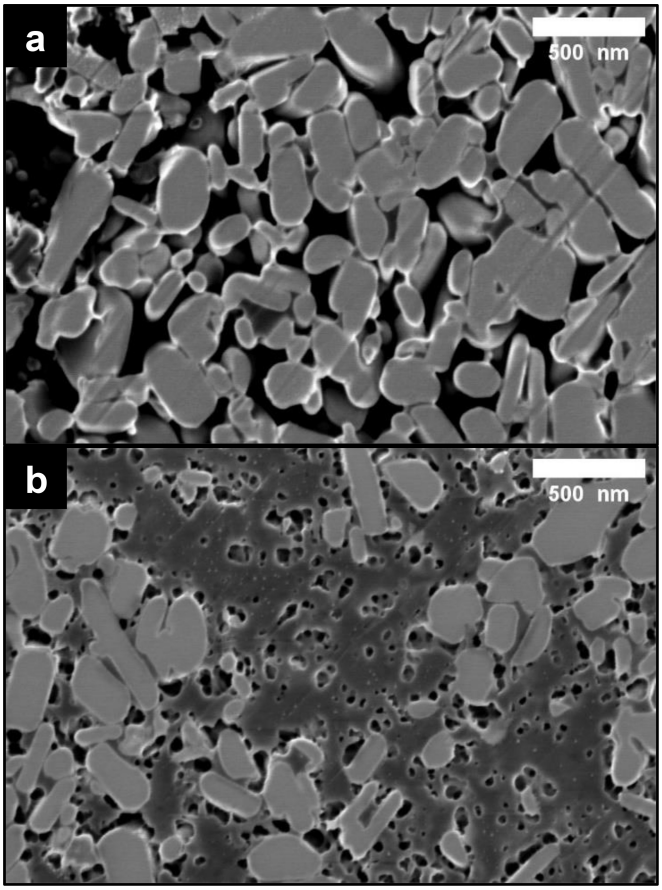

Figure 1. SEM micrographs of BIB polished cross-section of (a) pristine LFP electrode and (b) HE-50 wt%-LFP electrode before cycling.

Similar results were obtained for 45 wt%-LFP electrode (Figure S1) with a lower liquid electrolyte content. The HE-50 wt%-LFP sample, however, exhibited slightly higher porosity compared to the HE-45 wt%-LFP. The distribution of the pores was not uniform throughout the infused electrodes for both 50 wt%-LFP and 45 wt%-LFP samples, as shown in Figure S2–S3 at different magnifications. This phenomenon results from the interplay between the microstructure of the pristine electrode – which consists of active particles and voids (as shown in Figure S4 at different magnifications, and later filled by the uncured resin) – and the thermodynamics and kinetics of polymerization and phase separation processes. Due to the difference in thermal properties (thermal conductivity and specific thermal capacity) between the active material and the uncured resin, the polymerization and phase separation processes are expected to be non-uniform. Polymerization is a thermally initiated process at 90 °C. Thermodynamically, a large solid-liquid interface is not favorable. Thus, when the rate of polymerization is slow compared to the rate of phase separation, fewer solid-liquid interfaces are formed, thus larger phase domains of solid and liquid phase are expected, i.e. larger pores. The combined thermodynamic and kinetic considerations suggest that both the structural heterogeneity, and the interplay between polymerization and phase separation processes contribute to the observed pore distributions.

Figure S5 shows SEM images of HE-50 wt%-NMC before cycling at different magnifications. The results show that HE can also be effectively infused into NMC electrodes and incorporated between the micron-sized NMC particles when compared with the pristine NMC electrode (Figure S6). The HE-50 wt%-NMC present the expected highly porous structure with micro- to mesopores. As shown in typical images at different magnifications (Figure S5), the porosity in the HE between the micron-sized NMC particles is not uniform throughout the material. This non-uniformity is attributed to inherent inhomogeneities (active particles and voids) present in the pristine material. Similar results were obtained for HE-45 wt%-NMC (Figure S7). Also in the case of NMC electrodes, HE-50 wt%-NMC exhibits a slightly higher porosity compared to the HE-45 wt%-NMC, which is similar to the trend in HE-50 wt%-LFP and HE-45 wt%-LFP. This was expected since the liquid electrolyte acts effectively as a porogen, promoting the formation of a porous structure within the HE polymer phase.[14]

Stability of HEs at a Low C-Rate

The HE-infused electrodes underwent galvanostatic cycling for 10 cycles at C/20. The cycling data of the HE-50 wt%-LFP electrode half-cell are shown in Figure 2. The results of a reference sample containing only liquid electrolyte are shown in Figure S8 for comparison. The galvanostatic charge/discharge profile of both the reference and the HE-infused cells show stable cycling behavior. The voltage-time plot (Figure 2-a) of sample HE-50 wt%-LFP shows consistent voltage curves with the typical plateau expected when using LFP as electrode material. The HE-50 wt%-LFP electrode shows a specific capacity around 135 mAh/g (Figure 2-b) which is comparable with the specific capacity of the reference cell with liquid electrolyte, around 125 mAh/g (Figure S8). In both cells there is a minor decrease in capacity at increasing cycle number. The important finding in the present study is that both the HE-infused and the reference sample behave similarly. The similarity in specific capacity indicates that the HE can effectively allow lithium-ion transport and maintain the electrochemical performance of the LFP electrode. However, the overpotential for the HE-50 wt%-LFP electrode half-cell is higher compared to the reference. The observed difference is likely related to the additional resistance to ion transport in the presence of the polymer component in the HE.[14] This is caused by the reduced volume fraction of the liquid electrolyte, which is responsible for the ionic conduction. Moreover, the presence of very narrow pores (less than 10 nm) formed during the PIPS process further affects the ionic conductivity. It has been shown by the authors that in these narrow channels, the interactions between the electrolyte species and the polymer wall have a significant impact on ion mobility, thereby influencing the overall conductivity of the HEs.[14] Additionally, the polymer introduces extra tortuosity into the system, creating a more complex and longer path for ions to travel through.[28] This increased path length, or tortuosity, further impedes ion transport, as ions must navigate around and through the polymer structure rather than moving freely in a homogeneous liquid medium.[29]

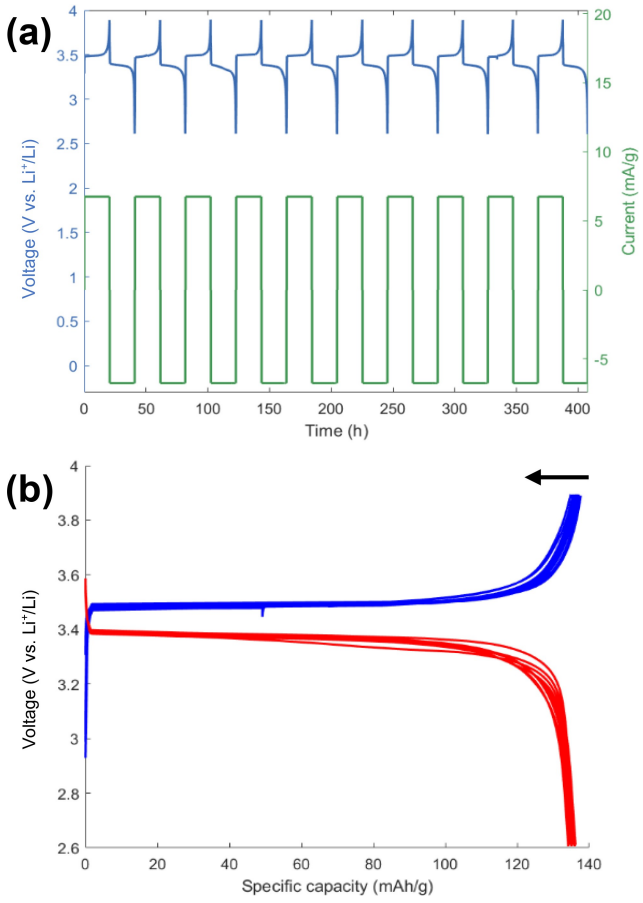

Figure 2. Galvanostatic charge/discharge profiles of HE-50 wt%-LFP electrode half-cell with applied current density of 6.75 mA/g (C/20): (a) voltage/current vs time plot and (b) voltage vs specific capacity plot, the arrow indicates the progression of cycles over time.

Similar results were obtained for 45 wt%-LFP electrode (Figure S9). For comparison, the first cycles of the HE-45 wt%-NMC electrode half-cell are shown in Figure S10. The galvanostatic charge/discharge profile also demonstrates a stable performance. The voltage-time plot exhibits consistent voltage curves with the typical NMC half-cell behavior, and the specific capacity is around 124 mAh/g. Figure S11 shows a comparison between the fourth cycle of the HE-45 wt%-NMC electrode half-cell and the reference one with only liquid electrolyte, the latter showing a specific capacity comparable to the former around 126 mAh/g. The galvanostatic charge/discharge profiles of both cells exhibit similar stable behavior. As in the case of LFP samples, the measured specific capacities are comparable and the overpotential is larger for the HE-infused electrode. It is important to note that the observed differences in the specific capacity for HE-infused electrodes half-cells are minor both for the LFP and the NMC sample series. This is explained by the fact that capacity is related to the accessibility to the active material. The accessibility is similar for the samples because they utilize the same LFP and NMC active materials and electrode designs, ensuring comparable lithium-ion intercalation and deintercalation processes. It is then expected that, at such a low C-rate, the capacities are similar. The electrochemical considerations presented here are intended to serve as a proof of concept, demonstrating the feasibility and potential of the HE-infused systems in all cases. To strengthen this observation, experiments were repeated with multiple cells, consistently yielding similar results.

The morphology of HE-infused electrodes after cycling were investigated with SEM. The results for HE-50 wt%-LFP electrode are shown in Figure 3. Upon cycling, the HE-infused electrode demonstrated stability in terms of its morphological characteristics, stressing the resilience of the phase separation structure. The pores seem to have remained intact, suggesting that the HE retained its structural framework, which is vital for its function. Similar results were obtained for HE-45 wt%-LFP electrode (Figure S12) with a lower liquid electrolyte content. The stable morphology throughout the material (see also different magnifications in Figure S13–S14) underlines the robustness of the HE formulation, which is crucial for the consistent performance of battery systems.

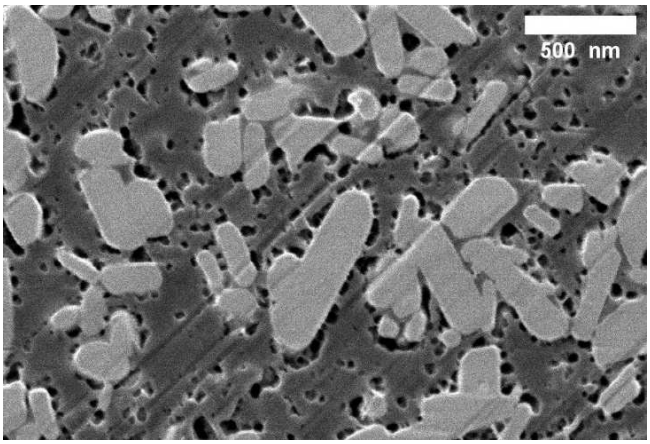

Figure 3. SEM micrographs of BIB polished cross-section of HE-50 wt%-LFP electrode after cycling.

The effectiveness of the infusion and PIPS of HE precursors and the subsequent stability of the formed HEs in the infused electrodes upon cycling were evident not only between the LFP particles but also in the cracks within LFP particles as shown in Figure 4. Similar results are observed also for cycled HE-45 wt%-NMC (Figure S15). It should be noted that there are two types of cracks present in the samples: 1) the cracks within the LFP particles that contain infused HE, indicating the effectiveness of the infusion, and 2) the cracks between the active particles and the HE, which may suggest damage to the HE due to volume changes. However, the extent of the second type of cracks is similar to that in the as-infused samples before cycling (highlighted with arrows in Figure S1 and Figure S7), indicating that these cracks most probably have been introduced during cell manufacturing or SEM specimen preparation. The results suggest that the HE-infused electrodes are robust under cycling.

Overall, the results indicate that the HE formulations under study not only are capable of permeating the electrode structures effectively, but also exhibit the requisite percolating liquid electrolyte for ion conductivity and stability upon electrochemical cycling. This affirms the potential of these HE systems in advanced battery applications where the interplay between morphology and performance is critical.

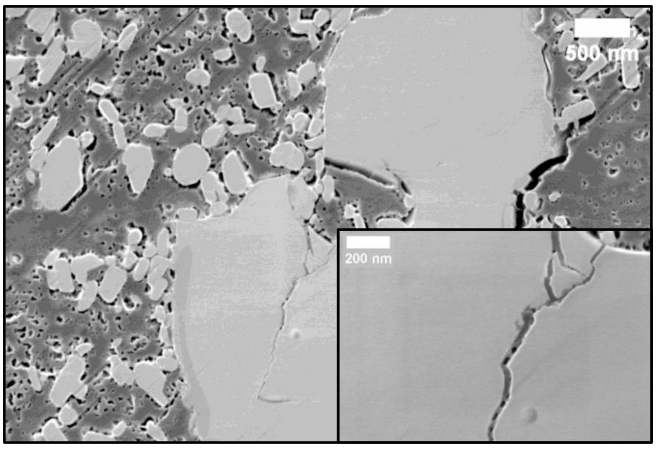

Figure 4. SEM micrographs of BIB polished cross-section of HE-45 wt%-LFP electrode particle after cycling. The inset shows details of the porous phase separated HE within LFP particle cracks.

Cycling Performance of the HE-Infused Electrode

The results of the galvanostatic cycling of the HE-infused half-cell further validate the electrochemical performance of the HE and the formation of an effective electrochemical interface. Figure 5 shows the capacity retention test results of the HE-50 wt%-LFP electrode half-cell where the capacity vs. cycle number is measured to evaluate how well the cell maintains its capacity after multiple cycles at different C-rates. The results of the reference sample with only liquid electrolyte are shown in Figure S16 for comparison. The specific capacity shows a stable value equal to 120 mAh/g at C/10 which drops to 100 mAh/g at C/5, which are comparable with the reference sample, with 122 mAh/g at C/10 and 105 mAh/g at C/5. Instabilities are seen at C/2 with a further capacity drop. Finally, the specific capacity goes back to 120 mAh/g when a C-rate of C/10 is applied again. The cycling data demonstrates overall stability in the specific capacities across various cycling rates. At higher cycling rates, a reduction in capacity is noted. At the highest C-rate (C/2), a significant difference emerged: the HE-infused sample exhibited a specific capacity of approximately 40 mAh/g, while the reference sample demonstrated a much higher value, around 80 mAh/g. This is consistent with the expected behavior due to limited transport properties in the electrolyte[30] as can be seen from results of the reference sample (Figure S16). Consistent specific capacities were observed at lower C-rates (C/10 and C/5) for the HE-infused sample compared with the reference cell with only liquid electrolyte. At lower C-rates, the importance of electrolyte conductivity decreases, thereby minimizing the impact of structural differences between the HE and the liquid

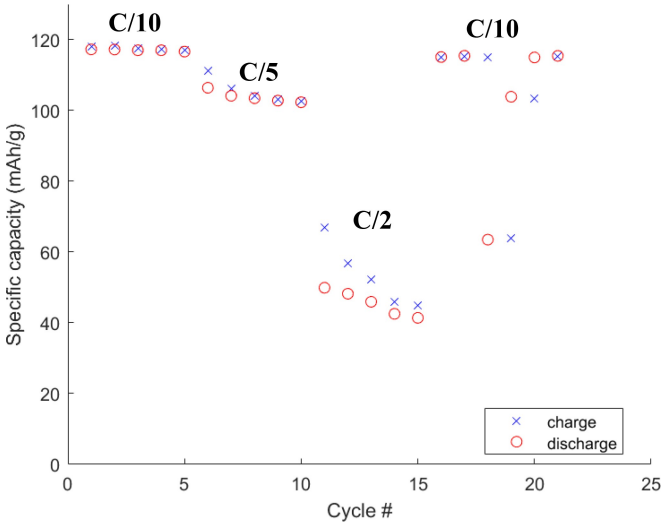

Figure 5. Capacity retention test of HE-50 wt%-LFP electrode half-cell with applied current densities of 13.5 mA/g (C/10), 27 mA/g (C/5) and 67.5 mA/g (C/2).

electrolyte. While other factors such as interfacial resistance could also potentially lead to the lower specific capacity of the HE at higher C-rates, further studies would be necessary to assess their role. Isolated instances where single data points deviate from the general trend are observed. These anomalies are, to a minor extent, present also in a few of the reference sample data points. Importantly, subsequent cycles following these deviations return to the expected performance, indicating the resilience and recovery capability of the system.

While the results in Figure 5 provide initial insights into the performance of the HE-infused electrodes, further long-term cycling tests are required to fully evaluate their stability and capacity retention over extended periods.

Future Perspectives

The exploration of HEs in combination with commercial cathodes demonstrates that the infusion and PIPS process does not compromise the stability, integrity, or electrochemical properties of the active cathode material. Additionally, the presence of the active material during polymerization does not alter the microstructural morphology or the electrochemical behavior of the HEs. This study opens promising avenues for future research and development in LIBs. In a parallel, still unpublished study, it has been demonstrated that during PIPS carbon black particles are likely to solely integrate into the polymer, thus, they can function as electron conductor within a composite electrode using HEs. One immediate next step is to investigate the integration of electrode active particles and carbon black within the HE matrix. If successful, this approach could provide combined functions of electrolyte and binder in a single step, offering an alternative to fluorinated binders and potentially minimizing some of the environmental impacts associated with battery manufacturing, as well as streamlining production and reducing costs. Looking ahead, studies that involve more realistic synthesis scenarios, where the active cathode material is present during the polymerization of the HE, could lead to many interesting research questions. For instance, will the incorporation of the active material into the polymer matrix influence the interfacial properties and the compatibility between the electrolyte and the active electrode material? This plays an important role in the overall performance, affecting both interfacial resistance and ion transport. Another challenge lies in controlling the dispersion of active material within the HE, which is crucial to ensuring uniform performance. Additionally, it is crucial to further optimize the PIPS process to achieve more uniform porosity and better control over the microstructure of the electrolyte. Investigating higher liquid electrolyte contents should also be considered, as achieving a one-pot manufacturing process to replace PVDF would likely require a much lower polymer content and higher liquid content. A higher liquid electrolyte content is also expected to address the relatively low charging rates in this study. Optimizing the liquid electrolyte content of the HEs and investigating the performance of HE-infused electrodes at higher C-rates and over extended cycling periods will be crucial to ensure their practical applicability in high-performance battery systems. Moreover, HE-infused electrodes may be used to improve the compatibility with solid-state electrolytes (SPEs), particularly in cases where achieving proper wetting of the active cathode material is challenging due to the high viscosity of traditional SPE resins. The use of HEs could improve the wetting properties, facilitating better infiltration into the active material and enhancing the interface between the solid electrolyte and the cathode.

Conclusions

This study has successfully demonstrated the potential of integrating HEs in commercial cathode framework with nano-sized and micron-sized active electrode materials. The infused electrodes exhibit well-defined phase-separated structures at different liquid electrolyte contents, indicating that PIPS can effectively proceed in such configurations. This study highlights the compatibility of HEs with conventional cathode and shows the potential of PIPS in battery manufacturing processes. By successfully integrating HEs with traditional cathodes, we developed working half-cells that could potentially improve the safety of current battery technologies. The HE-infused electrodes maintain their morphology after cycling and show electrochemical performances comparable with reference half-cells with only liquid electrolyte. While the preliminary cycling results suggest promising stability, further long-term cycling tests are needed to fully assess the reliability of HEs synthesized via the PIPS process. Finally, using HEs in commercial LIBs could potentially enable novel production methods and eliminate the need for the conventional PVDF binder.

Acknowledgements

The Swedish Energy Agency (grant #48488) is gratefully acknowledged for financial support.

Conflict of Interests

The authors declare no conflict of interest.

Data Availability Statement

The data that support the findings of this study are available from the corresponding author upon reasonable request.

Keywords: Electrochemistry · Interfaces · Lithium-Ion Batteries · Multifunctional Materials · Polymer Electrolytes

[1] M. Armand, P. Axmann, D. Bresser, M. Copley, K. Edström, C. Ekberg, D. Guyomard, B. Lestriez, P. Novák, M. Petranikova, W. Porcher, S. Trabesinger, M. Wohlfahrt-Mehrens, H. Zhang, *J. Power Sources* **2020**, *479*, DOI: 10.1016/j.jpowsour.2020.228708.

[2] M. Armand, J. M. Tarascon, *Natur* **2008**, *451*(7179), 652–657, DOI: 10.1038/451652a, 2008/02/01.
[3] A. Yoshino, *Bull. Chem. Soc. Jpn.* **2022**, *95*(1), 195–197, DOI: 10.1246/bcsj.20210338.
[4] M. Winter, R. J. Brodd, *Chem. Rev.* **2004**, *104*(10), 4245–4270, DOI: 10.1021/cr020730k, 2004/10/01.
[5] K. W. Beard, *Linden's Handbook of Batteries, Fifth Edition* **2019**, McGraw Hill LLC, 3–23.
[6] W. Lee, S. Muhammad, C. Sergey, H. Lee, J. Yoon, Y. M. Kang, W. S. Yoon, *Angew. Chem. Int. Ed. Engl.* **2020**, *59*(7), 2578–2605, DOI: 10.1002/anie.201902359,2020/10/02.
[7] S. Li, K. Wang, G. Zhang, S. Li, Y. Xu, X. Zhang, X. Zhang, S. Zheng, X. Sun, Y. Ma, *Adv. Funct. Mater.* **2022**, *32*(23), DOI: 10.1002/adfm.202200796.
[8] J. Kalhoff, G. G. Eshetu, D. Bresser, S. Passerini, *ChemSusChem* **2015**, *8*(13), 2154–2175, DOI: 10.1002/cssc.201500284.
[9] T. Minato, T. Abe, *Prog. Surf. Sci.* **2017**, *92*(4), 240–280, DOI: 10.1016/j.progsurf.2017.10.001, 2017/12/01.
[10] X. Yu, A. Manthiram, *Energy Environ. Sci.* **2018**, *11*(3), 527–543, DOI: 10.1039/C7EE02555F.
[11] H. Jia, W. Xu, *Trends Chem.* **2022**, *4*(7), 627–642, DOI: 10.1016/j.trechm.2022.04.010, 2022/07/01.
[12] M. Piglowska, B. Kurc, M. Galinski, P. Fuc, M. Kaminska, N. Szymlet, P. Daszkiewicz, *Mater.* **2021**, *14*(22), 6783, DOI: 10.3390/ma14226783.
[13] M. Zhu, J. Wu, Y. Wang, M. Song, L. Long, S. H. Siyal, X. Yang, G. Sui, *J. Energy Chem.* **2019**, *37*, 126–142, DOI: 10.1016/j.jechem.2018.12.013.
[14] M. Cattaruzza, Y. Fang, I. Furó, G. Lindbergh, F. Liu, M. Johansson, *J. Mater. Chem. A.* **2023**, *11*(13), 7006–7015, DOI: 10.1039/D3TA00250K.
[15] N. Ihrner, W. Johannisson, F. Sieland, D. Zenkert, M. Johansson, *J. Mater. Chem. A* **2017**, *5*(48), 25652–25659, DOI: 10.1039/c7ta04684g.
[16] N. Shirshova, A. Bismarck, E. S. Greenhalgh, P. Johansson, G. Kalinka, M. J. Marczewski, M. S. P. Shaffer, M. Wienrich, *J. Phys. Chem. C* **2014**, *118*(49), 28377–28387, DOI: 10.1021/jp507952b.
[17] S. Emilsson, V. Vijayakumar, J. Mindemark, M. Johansson, *Electrochim. Acta* **2023**, *449*, DOI: 10.1016/j.electacta.2023.142176.
[18] S. A. Chopade, J. G. Au, Z. Li, P. W. Schmidt, M. A. Hillmyer, T. P. Lodge, *ACS Appl. Mater. Interfaces.* **2017**, *9*(17), 14561–14565, DOI: 10.1021/acsami.7b02514, 2017/05/03.
[19] S. A. Chopade, S. So, M. A. Hillmyer, T. P. Lodge, *ACS Appl. Mater. Interfaces.* **2016**, *8*(9), 6200–6210, DOI: 10.1021/acsami.5b12366, 2016/03/09.
[20] L. D. McIntosh, M. W. Schulze, M. T. Irwin, M. A. Hillmyer, T. P. Lodge, *Macromol.* **2015**, *48*(5), 1418–1428, DOI: 10.1021/ma502281k.
[21] M. W. Schulze, L. D. McIntosh, M. A. Hillmyer, T. P. Lodge, *Nano Lett.* **2014**, *14*(1), 122–126, DOI: 10.1021/nl4034818.
[22] W. B. Hawley, J. Li, *J. Energy Storage* **2019**, *25*, 100862, DOI: 10.1016/j.est.2019.100862, 2019/10/01.
[23] B. Chen, Z. Zhang, M. Xiao, S. Wang, S. Huang, D. Han, Y. Meng, *ChemElectroChem* **2024**, *n/a(n/a)*, e202300651, DOI: 10.1002/celc.202300651.
[24] D. Zenkert, R. Harnden, L. E. Asp, G. Lindbergh, M. Johansson, *Composites Part B* **2024**, *273*, 111240, DOI: 10.1016/j.compositesb.2024.111240, 2024/03/15.
[25] L. E. Asp, K. Bouton, D. Carlstedt, S. Duan, R. Harnden, W. Johannisson, M. Johansen, M. K. G. Johansson, G. Lindbergh, F. Liu, K. Peuvot, L. M. Schneider, J. Xu, D. Zenkert, *Advanced Energy and Sustainability Research* **2021**, *2*(3), 2000093, DOI: 10.1002/aesr.202000093.
[26] R. Chaudhary, A. Chetry, J. Xu, Z. Xia, L. E. Asp, *Adv. Sci.* **2024**, *n/a(n/a)*, 2404012, DOI: 10.1002/advs.202404012.
[27] K. Bouton, L. Schneider, D. Zenkert, G. Lindbergh, *Compos. Sci. Technol.* **2024**, *256*, 110728, DOI: 10.1016/j.compscitech.2024.110728, 06/25/2024.
[28] S. Duan, M. Cattaruzza, V. Tu, R. M. Auenhammer, R. Jänicke, M. K. G. Johansson, F. Liu, L. E. Asp, *Commun. Mater.* **2023**, *4*(1), 49, DOI: 10.1038/s43246-023-00377-0.
[29] I. V. Thorat, D. E. Stephenson, N. A. Zacharias, K. Zaghib, J. N. Harb, D. R. Wheeler, *J. Power Sources* **2009**, *188*(2), 592–600, DOI: 10.1016/j.jpowsour.2008.12.032, 2009/03/15.
[30] R. A. Huggins, *Advanced Batteries: Materials Science Aspects* **2008**, 433–440.

Version of record online: January 31, 2025